Accepted version of: Heinrich Edgar Arnold Laue and Warren Paul du Plessis, “Design and Analysis of a Proof-of-Concept Chequered-Network Compressive Array,” in *IEEE Transactions on Antennas and Propagation*, vol. 70, no. 9, pp. 7546–7555, Sep. 2022. DOI: 10.1109/TAP.2022.3188531

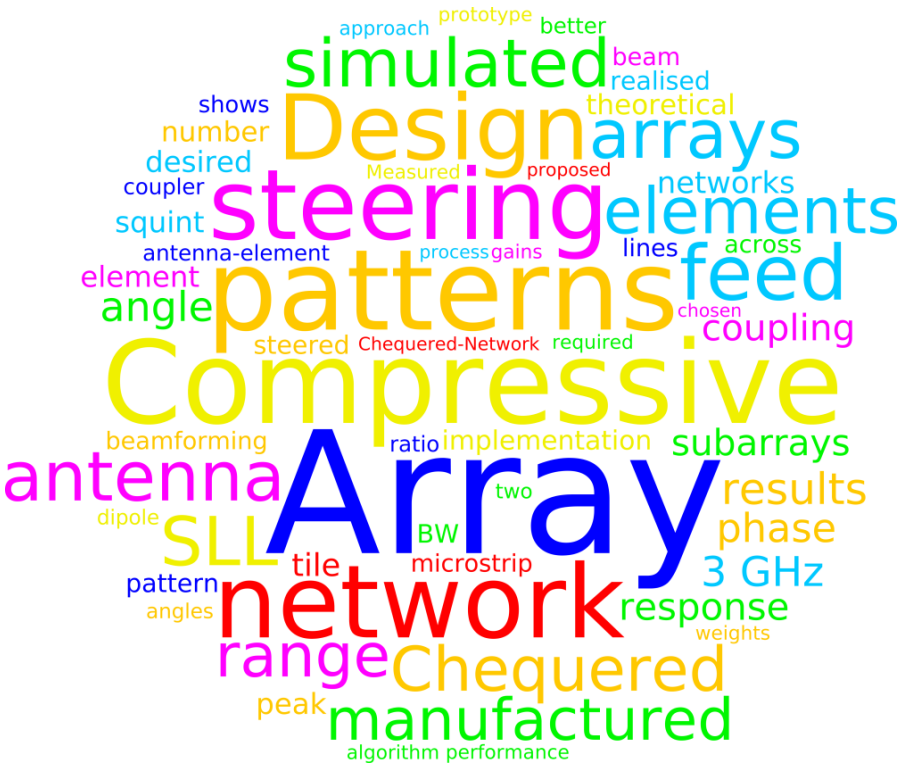

Design and Analysis of a Proof-of-Concept Chequered-Network Compressive Array

Heinrich Edgar Arnold Laue, *Member, IEEE,* and Warren Paul du Plessis, *Senior Member, IEEE*

***Abstract*—Compressive arrays have recently been proposed as a new technique for reducing the number of controls in a beamforming system for a given array aperture, promising improved performance over existing thinned-array and subarray techniques. Chequered networks, feed networks consisting of interconnected couplers and fixed phase shifters, have been suggested for realising the required overlapped subarrays. Although a chequered network has previously been implemented in microstrip, an integrated compressive array, comprising both the antenna elements and the feed network, is required to demonstrate the practical feasibility of such systems. Results for the first successfully manufactured chequered-network compressive array with integrated antenna elements are presented, thereby showing that compressive arrays are promising for use in a variety of real-world beamforming applications. Analysis of the results shows that steered-beam squint is a greater issue than previously assumed, and design guidelines are presented for minimising the risk of excessive steered-beam squint in manufactured compressive arrays.**

***Index Terms*—Compressive arrays, chequered networks, antenna feeds, subarray feeds, beam steering, phased arrays**

I. Introduction

BEAMFORMING antenna arrays are used to transmit or receive signals in various directions while the physical array remains stationary [2]. Electronic controls steer the array in different directions [2]. These dynamic beamforming controls are implemented in hardware using phase shifters, in software using transmitters/receivers at the antenna elements, or using a compromise between these two approaches [3].

Reduced-control arrays limit the number of controls for a given antenna aperture in order to reduce cost, size and/or weight [2], [4]–[7]. Thinned arrays are formed by taking a filled array and removing or disabling some of the elements [2], [8]–[10]. Sparse arrays are similar to thinned arrays, but the element locations are not restricted to an underlying grid [11], [12]. Subarrays combine the signals from multiple antenna elements [2], [6], [7]. If some or all of the antenna elements are shared between the subarrays, they are referred to as partially and completely overlapped subarrays, respectively. Feed networks are used to weigh and combine the antenna-element signals using splitters and combiners [13], [14], directional couplers [5], [7], [15], [16], lenses [2], [17], or radio-frequency integrated circuits (RFICs) [18].

The compressive-array approach is a generalisation of reduced-control techniques with fixed antenna layouts [4]. A complex-valued feed-network response matrix $\mathbf{\Phi}$ describes how the antennas are combined to form the subarrays. Generally, compressive arrays are completely overlapped subarray systems. However, placing appropriate constraints on $\mathbf{\Phi}$ allows other topologies to be represented [4], [19].

Algorithms have been proposed for optimising compressive arrays based on radiation-pattern requirements or direction-finding (DF) performance [4], [19]. Allowing the weights for combining the antenna elements to be chosen arbitrarily leads to improved performance over conventional reduced-control techniques, generally at the expense of a more complicated feed network [5]. However, this means that the algorithms do not consider hardware constraints when choosing the weights for combining the antenna elements.

Compressive arrays have been shown to have theoretically superior performance to weighted thinned arrays, conventional uniform linear arrays (ULAs) for the same number of controls, and dual-transform completely overlapped subarray systems [4]. A novel theoretical design for a circular beamforming array showed that a null can be implemented in hardware, thereby suppressing an interferer before reaching the receivers [4].

A planar feed network consisting of tiles connected in a chequered pattern has been proposed for implementing arbitrary feed networks, where each tile consists of a coupler and two fixed phase shifters [5]. A prototype chequered feed network has been realised successfully in microstrip [5]. However, no the details of the hardware implementation were given and the antenna elements were not included in the design, so the chequered network could not be evaluated in terms of resulting radiation patterns. Measured results were presented for the feed-network response, but the relationship between the accuracy of the feed-network implementation and the accuracy of the resulting antenna patterns was not quantified.

This paper describes the first successfully manufactured chequered-network compressive array. The prototype comprises a chequered feed network in microstrip along with printed dipole antenna elements. The narrowband 3-GHz prototype has four antenna elements and two subarrays, yet manages to achieve a beam that is steerable across ±10° with a beamwidth comparable to that of a four-element ULA with uniform excitations. The entire compressive array was

Manuscript received 1 October 2021; revised 10 March 2022 and 2 May 2022; accepted 23 May 2022.

This work is based on a chapter in [1].

The authors are with the Department of Electrical, Electronic and Computer Engineering, University of Pretoria, Pretoria 0002, South Africa (e-mail: hlaue@ieee.org; wduplessis@ieee.org)

Color versions of one or more of the figures are available online at http://ieeexplore.ieee.org.

Digital Object Identifier 10.1109/TAP.2022.3188531

manufactured on a single double-sided printed circuit board (PCB), has no crossing transmission lines, and did not require tuning after manufacturing.

The proof-of-concept prototype demonstrates the practical feasibility of chequered-network compressive arrays in several important ways. Costly full-wave optimisation is only required at tile level, making the proposed approach computationally scalable. Successful use is made of embedded antenna-element patterns during pattern synthesis, demonstrating that compressive arrays are not restricted to arrays with identical antenna-element patterns. The prototype also highlights areas where manufacturing has the greatest potential impact on performance. Analysis of the results shows that steered-beam squint is a much greater issue than previously assumed on the basis of separate manufacture and testing of the antenna elements and the feed network. This squint is particularly sensitive to manufacturing tolerances and needs to be addressed during the design phase. Care must be taken in how the steering range is specified since both sidelobe level (SLL) and steered-beam squint tend to worsen at extreme steering angles.

The description of this work will start with an overview of compressive arrays and chequered networks in Section II. The design of the prototype compressive array will then be described in Section III, including a design methodology, prototype specifications, antenna-element design, feed-network design, and microstrip feed-network implementation. Simulated and measured results are presented in Section IV and compared to the theoretical results. Finally, a summary is provided in Section V.

II. Background

The proof-of-concept array described below is a compressive array, so compressive arrays are briefly introduced in Section II-A. Approaches to implementing completely overlapped feed networks are briefly considered in Section II-B, with the emphasis on the chequered network that is used in the proof-of-concept array.

A. Compressive Arrays

Fig. 1 illustrates a compressive array with $N = 4$ antenna elements and $M = 2$ subarrays. The array will be considered on receive below, although the same principles apply on transmit by reciprocity.

For each subarray m, unique complex weights are applied to all antenna-element signals x_n before being summed to form the subarray output y_m. The subarray weights $\phi_{m,n}, n \in 1, \ldots, N$ form the rows of the feed-network response matrix $\mathbf{\Phi}$. The $M \times 1$ signal vector at the subarrays, $\mathbf{y}$, is related to the $N \times 1$ antenna-element signal vector $\mathbf{x}$ via $\mathbf{y} = \mathbf{\Phi x}$. The subarray signals y_m are weighted by complex beamforming weights w_m before being summed to form the steered pattern. While $\mathbf{\Phi}$ is fixed, the beamforming weights w_m are dynamic and may be implemented in hardware or in software [4]. More advanced beamforming algorithms such as minimum variance distortionless response (MVDR) may also be applied to a digitised $\mathbf{y}$ on reception [1], [20].

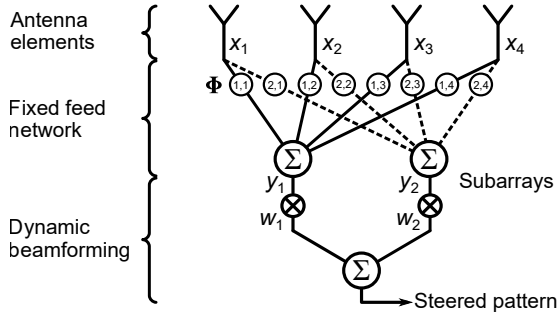

Fig. 1. An illustration of a compressive array with $N = 4$ antenna elements and $M = 2$ subarrays.

Various approaches to designing compressive feed-network responses exist [1], [4], [19]–[21]. A suboptimal approach is forming $\mathbf{\Phi}$ from a random distribution [1], [20], [21]. For DF, a least-squares pattern-matching approach has been proposed, as well as an optimisation procedure based on the Cramér-Rao bound (CRB) [19]. A recent algorithm [4] minimises the worst SLL as the main beam is scanned across a given steering range, with optional sidelobe-shaping constraints independent of steering angle. This algorithm is used in this paper because of its ability to control beamwidth and minimise SLL – key parameters in antenna-array design [2]. Nevertheless, the proposed implementation approach is valid for any desired response $\mathbf{\Phi}$.

B. Completely Overlapped Feed Networks

Completely overlapped subarrays make use of feed networks that allow each subarray output to be connected to each antenna element, thereby sharing the entire array aperture between all of the subarrays.

Various techniques exist for implementing completely overlapped feed networks in hardware [2], [5], [7], [16], [22]. Dual-transform arrays make use of an $N \times N$ Butler matrix with its central beam outputs connected to an $M \times M$ Butler matrix, with the smaller matrix often implemented in software [2], [7]. The chess network of Skobelev connects branch-line couplers in a chequered pattern to synthesise subarray patterns that differ only in their phase centres [7]. The chequered network is an extension of the Skobelev chess network, where couplers in the same row are not required to be equivalent, and fixed phase shifts are introduced between the couplers [5]. The feed network subsequently proposed by Hirokawa *et al.* also utilises a network of branch-line couplers and phase shifts, but focuses on beam-switching applications where the number of subarrays equals the number of antenna elements [16]. Coherently radiating periodic structures (CORPS) are reduced-control feed networks for limited-scan applications that make use of a network of splitters and combiners to reduce the number of active phase shifters and variable amplifiers required to perform beamforming [22].

The primary advantage of chequered networks over other techniques is that they allow completely arbitrary overlapped feed-network responses to be realised, making them particularly suitable for applications where pattern control is the

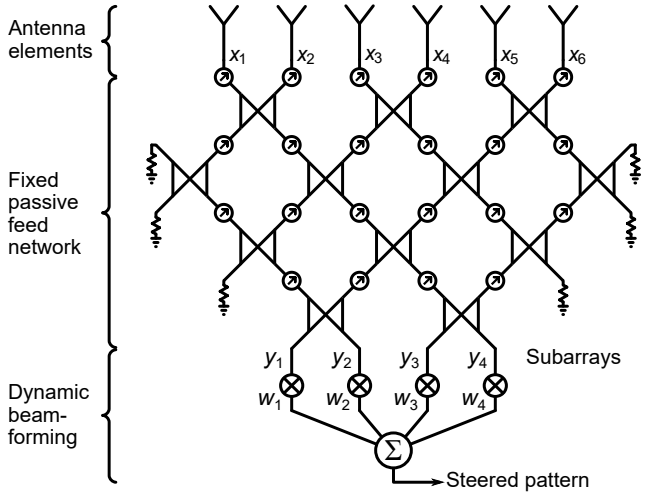

Fig. 2. A chequered-network compressive array with $N = 6$ antenna elements, $M = 4$ subarrays, and four tile rows. Adapted from [5].

highest priority [5]. The disadvantage is that this freedom comes at the potential expense of a more complicated feed network. The chequered-network technique was validated by approaching the standard Butler-matrix implementation when given the same target response [5]. The ability to implement arbitrary feed-network responses was illustrated by designing a feed network that allowed three independently specified non-scanning arrays, namely $\text{cosec}^2 \cos$, flat-topped, and Chebyshev arrays, to share the same eight-element aperture [5].

A chequered-network compressive array with $N = 6$ antenna elements, $M = 4$ subarrays, and four tile rows is illustrated in Fig. 2 [5]. The signals undergo amplitude and phase alterations along the various paths, which work together to realise the arbitrary complex-valued response $\mathbf{\Phi}$. Each new row adds to the number of signal paths, thereby increasing the degrees of freedom. Typically, each subarray port must have at least two signal paths to each antenna element [5].

The chequered-network layout is entirely planar, thereby avoiding crossovers and their associated implementation challenges [23]. Each tile consists of a coupler with fixed phase shifters at its upper ports. Couplers must have adjacent through and coupled ports, e.g. branch-line couplers, to avoid crossing transmission lines. The coupling ratio is defined as to the ratio of square-root power delivered to the through port to that delivered to the coupled port for a given stimulus.

The parameters that implement a desired $\mathbf{\Phi}$ are found via optimisation [5]. A chequered network with a small range of coupling ratios around 0 dB is less challenging to implement successfully in hardware and is therefore preferable. The minimum and maximum coupling ratios can be constrained [5]. The range of coupling ratios can also be minimised by repeating the optimisation with ever-stricter constraints. The phase shifts can be minimised in a similar fashion.

III. Design and Implementation

This section starts by considering the specifications of the proof-of-concept compressive array in Section III-A, and then moves on to describe the design of the dipole array in Section III-B as the array is required to synthesise the feed network. This feed-network synthesis is then outlined in Section III-C along with the process to implement this desired response using a chequered network. Finally, the microstrip implementation of the feed network is presented in Section III-D.

A. Design Specifications

The chosen application for the prototype is a beamforming array with a limited steering range. Four antenna elements and two subarrays were chosen. Obtaining reasonable performance from such a small array would require all the available degrees of freedom to be exploited, making it a good test of the capabilities of the compressive-array approach.

The specifications chosen for the proof-of-concept compressive array are listed below.

1) The compressive array should operate at 3 GHz. This frequency allows reasonably compact distributed circuit implementation while still maintaining dimensions large enough to be manufactured using standard techniques.
2) The steering range should be $|\theta_s| \leq 10°$ (rounded to $|\sin(\theta_s)| \leq 0.175$), a typical range for limited-steering applications [6].
3) The start of the SLL region should be at $\sin(\theta) = 0.35$. This results in an SLL similar to that of an uniform-excitation four-element ULA with isotropic elements with spacings of half a wavelength.
4) The voltage standing wave ratios (VSWRs) of the subarrays should be better than 2:1 and the isolation between the subarray ports better than 10 dB.
5) Due to cost limitations, the compressive feed network and antenna array should fit on a single sheet of double-sided Rogers RO4003C substrate of dimensions 272 mm by 196 mm (the usable space on a 9" by 12" sheet).

B. Dipole Array Design

The design of the embedded antenna elements was performed in simulation using Computer Simulation Technology (CST) Microwave Studio 2018. The chosen antenna technology is a printed dipole with an integrated balun since it is easy to implement on double-sided subtrate [24], [25].

The chosen element spacing was 0.64 wavelengths. This ensures that the main-beam region of an ambiguity does not enter the visible region up to a steering angle of $\sin(\theta_s) = 0.2125$ or $\theta_s = 12.3°$, slightly wider than the steering range of interest.

Fig. 3 shows the simulated embedded element gain patterns, and Fig. 4 shows the worst-case return loss and isolation across all the elements. The elements have peak gains ranging from 4.3 dBi to 4.8 dBi. Across $|\theta| \leq 10°$, the gain of each individual element varies by at most 0.3 dB. The VSWRs are equal to 2:1 (a return loss of 9.5 dB) or better from 2.82 GHz to 3.36 GHz, giving an impedance bandwidth of 17%. The isolation between all elements is better than 17.2 dB across this range. The return losses at 3 GHz are 46.6 dB or better and the isolations at 3 GHz are 19.5 dB or better.

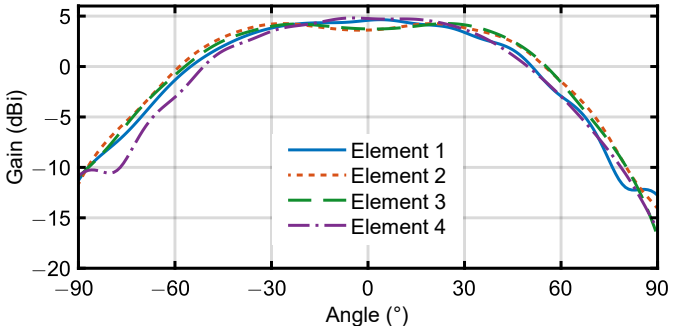

Fig. 3. Simulated embedded dipole element azimuth gain patterns at 3 GHz.

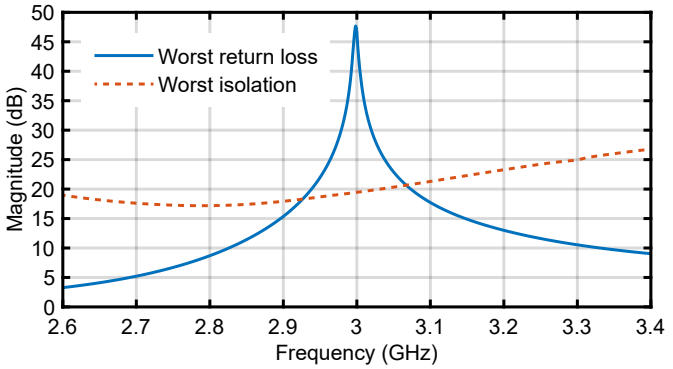

Fig. 4. Simulated worst-case return loss and isolation across all dipole elements.

The simulated embedded element patterns were used to design the feed-network response as described in Section III-C. This shows that the compressive-array design algorithm [4] can use non-identical embedded element patterns, including those from unconventional antenna-element layouts, for example where the mutual coupling between antenna elements varies due to uneven spacings.

C. Feed-Network Response and Chequered-Network Design

The feed-network response $\mathbf{\Phi}$ was designed using the compressive-array design algorithm [4] for the specifications listed above with the simulated embedded element patterns in Fig. 3. The element patterns were only specified and the SLL only calculated across $\theta \in [-90°, 90°]$ since the simulated element patterns suggested that the patterns outside $\theta \in [-90°, 90°]$ were sufficiently suppressed due to the ground-plane reflector behind the printed dipole elements. The measured results in Section IV-B validate this assumption.

Since the SLL of a compressive array typically deteriorates rapidly beyond the steering range (e.g. [4, Fig. 7]), a slightly wider steering range of $|\sin(\theta_s)| \leq 0.2$ or $|\theta_s| \leq 11.5°$ was passed to the algorithm. The sum of the subarray pattern powers (see Section IV-D) was constrained to be within ±0.1 dB across the steering range [4, eq. (15)–(16)]) as the SLL deteriorated rapidly when the constraint was reduced below this value. The algorithm was run 20 times and all 20 designs achieved an SLL of −11.3 dB. All 20 designs were therefore considered as candidates for implementation in chequered feed networks.

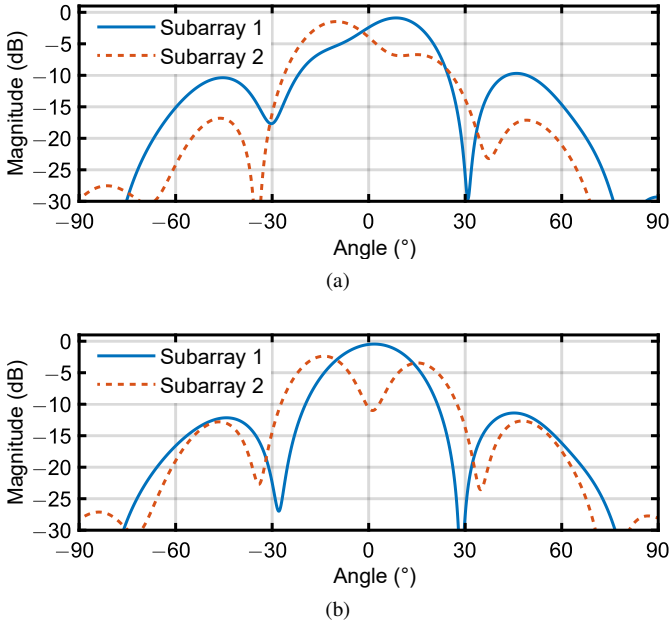

Fig. 5. Resulting subarray patterns from the compressive-array design algorithm for (a) design 10 and (b) design 15.

The feed-network responses were implemented as chequered networks using the chequered-network design algorithm [5]. The chequered networks were required to implement the desired responses with magnitude and phase tolerances of ±0.1 dB and ±1°, roughly an order of magnitude stricter than the expected accuracy of the hardware implementation [5]. Further tightening these tolerances would make it more difficult to find a practical solution without significantly improving the performance of the manufactured circuit.

The range of phase shifts was constrained to $\psi \in [-260°, -140°]$. The upper bound corresponds to the approximate minimum length of transmission line required to connect two couplers for the chosen tile size. The lower bound is the approximate longest transmission line that would fit on a tile of the chosen size.

The minimum and maximum coupling-ratio constraints were tightened with equal priority to minimise the range of coupling ratios in the final design [5]. Couplers from the initial solution with coupling ratios above 20 dB were shorted (replaced with 90° transmission lines [5]), and 20 trial points were used in each run of the MATLAB MultiStart algorithm [5].

All 20 compressive feed networks were successfully synthesised as chequered networks. The smallest coupling-ratio range (the difference in decibels between the largest and smallest coupling ratio for a given design) was 3.2 dB in design 15, the median coupling-ratio range 9.5 dB, and the largest coupling-ratio range 13.1 dB. The smallest phase-shift range for any one design was 54° again in design 15, the median phase-shift range 87°, and the largest phase-shift range 120°.

Fig. 5 shows the subarray patterns for the two designs with the smallest coupling-ratio ranges, namely design 10 (7.2 dB) and design 15 (3.2 dB). Design 10 has two beams pointing in opposite directions, while design 15 has one subarray with a

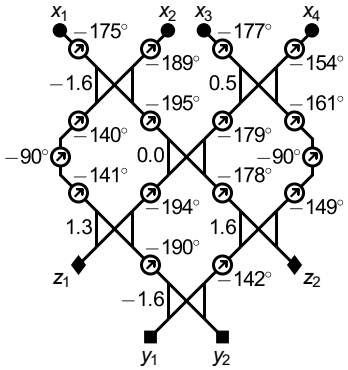

Fig. 6. Chequered network obtained for design 15. Coupling ratios in decibels appear to the left of the couplers.

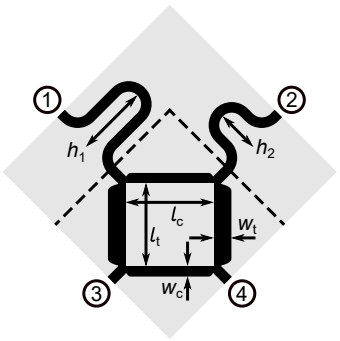

Fig. 7. Microstrip implementation of a single chequered-network tile with optimisation parameters indicated. Each side is 40 mm long. Tile port numbers are encircled. Dashed lines indicate where the tile is cropped for the optimisation of the coupler.

single main lobe near broadside, and one subarray with two lobes to the left and right of broadside and low gain near broadside. These two designs show striking similarities to two common types of monopulse array patterns, namely squinted-beam monopulse patterns and sum-and-difference monopulse patterns [26] . The compressive-array design algorithm is thus shown to approach well-established techniques for limited-scan direction-of-arrival (DoA) estimation. Therefore, the algorithm can also be expected to obtain good results for larger systems and systems with unconventional requirements for which designs do not yet exist.

Design 15 was chosen since it had the smallest coupling-ratio and phase-shift ranges. The resulting chequered-network design is shown in Fig. 6. The coupling ratios range from −1.6 dB to 1.6 dB and the phase shifts from −195° to −140°. This design has the added benefit of transferring no power to matched loads on transmit, making it lossless on transmit [27], [28].

Although similar patterns can be realised by a monopulse comparator network with rat-race couplers [26], the advantage of the chequered-network configuration is that the circuit implementation is entirely planar, with the antenna-element ports ordered correctly for direct connection to the antenna elements without any crossovers.

D. Microstrip Implementation of the Chequered Network

Microstrip was chosen to implement the chequered network since it can be manufactured easily on double-sided PCB. The chosen substrate was Rogers RO4003C with a process dielectric constant of 3.38 and a height of 0.81 mm [29]. In simulation, the recommended design value of 3.55 for the dielectric constant was used.

The proposed microstrip circuit with associated parameters for a single tile is shown in Fig. 7, where the tile is square with sides being 40 mm long. The circuitry consists of a single-section branch-line coupler and two meandered transmission lines with variable lengths. Since the application is a narrow-band system, meandered transmission lines were chosen to implement the phase shifts due to their simplicity.

Large coupling ratios lead to wide microstrip lines with potentially significant discontinuities at the coupler junctions. Discontinuities are therefore compensated for using constant-impedance tapers [30].

The first step in the optimisation of a tile is to crop the tile as illustrated by the dashed lines in Fig. 7, leading to a coupler circuit with horizontal and vertical symmetry. The lengths and widths of the coupler arms are optimised for the following goals.

1) The coupling ratio, given by $|S_{31}|/|S_{41}|$, must equal the desired coupling ratio.
2) S_{11} is minimised at 3 GHz which, by symmetry, ensures that all junctions are matched.
3) The phase difference $\angle S_{41} - \angle S_{31}$ (the phase length of the branch lines) must equal $-90°$ as assumed in the theoretical tile model. This enables accurate phases to be realised when the meandered lines are included.
4) S_{21} is minimised at 3 GHz to maintain isolation between ports 1 and 2, and between ports 3 and 4 by symmetry.

After optimising the coupler in isolation, the meandered lines are included and their heights are optimised to implement the desired phase shifts ψ_1 and ψ_2, giving $\angle S_{31} = \psi_1 - 90°$ and $\angle S_{42} = \psi_2 - 90°$. Matched terminations at ports z_1 and z_2 were realised using 50 Ω 0805 surface-mount resistors that were connected to the ground plane by means of vias.

Fig. 8(a) shows the complete microstrip circuit with all the tiles connected. The transmission lines that connect the upper tiles to antenna elements 2 and 3 have the same phase length as the transmission lines connected to elements 1 and 4.

Optimising an assembled compressive array would require vastly more computational resources than optimising individual tiles. The assembled compressive array produced acceptable results in simulation and thus no further optimisation was necessary. This suggests that it will be feasible to design even large chequered networks using full-wave simulation, since tiles can be optimised individually and in parallel.

IV. Results

Fig. 8(b) shows a photograph of the manufactured and assembled compressive array. The substrate and subminiature version A (SMA) connectors were held together using 10-mm wide square brass rods on both sides of the circuit.

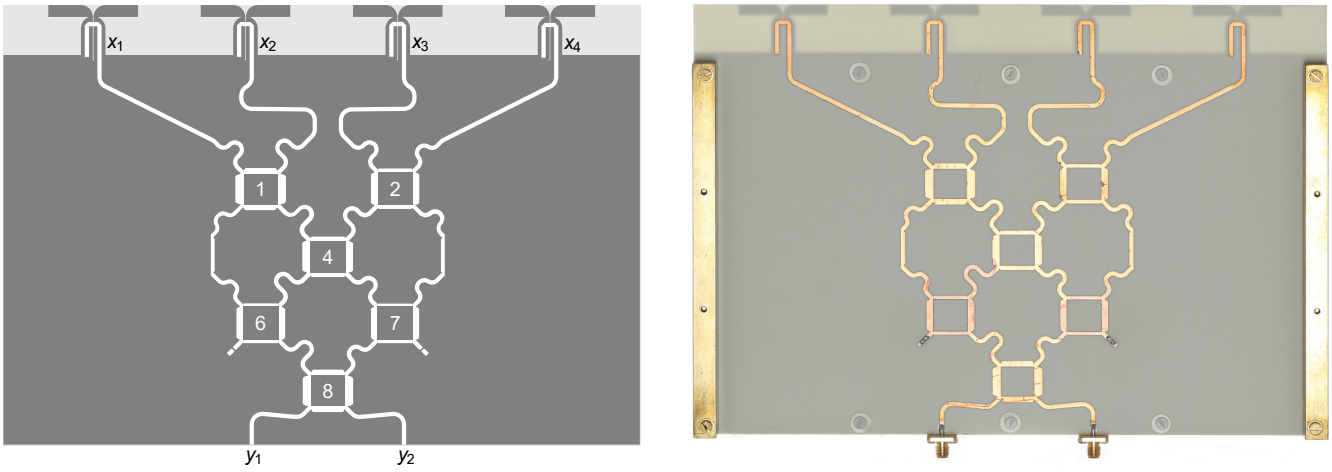

(a) (b)

Fig. 8. (a) Two-layer microwave circuit for the complete compressive array, with tile and port numbers indicated. Top-layer copper and coupler numbers are shown in white and bottom-layer copper in dark grey. The substrate measures 268 mm by 185 mm. (b) Photograph of the manufactured compressive array.

The compressive array was manufactured by a local PCB manufacturer in accordance with IPC-6012 Class 2 [31]. The compressive array patterns were measured at the Compact Antenna Test Range (Centre for Electromagnetism) at the University of Pretoria, South Africa.

A. Scattering Parameter Results

Fig. 9 shows the simulated and measured scattering parameters of the assembled compressive array.

The return losses and isolation of the simulated array are all better than 17.1 dB at 3 GHz. The simulated array has VSWRs of 2:1 (a return loss of 9.5 dB) or better from 2.77 GHz to beyond 3.4 GHz, but the isolation is better than 10 dB only up to 3.35 GHz. This gives a combined impedance and isolation bandwidth of 19%.

The return losses and isolation of the manufactured array are better than 17.7 dB at 3 GHz. The manufactured array has VSWRs of 2:1 or better from 2.84 GHz to 3.28 GHz for an impedance bandwidth of 14%, and the isolation across this range is better than 12.3 dB. Considering the resonant frequencies of S_{12} and S_{22}, there appears to be an upward frequency shift of about 70 MHz from the simulated to the manufactured results.

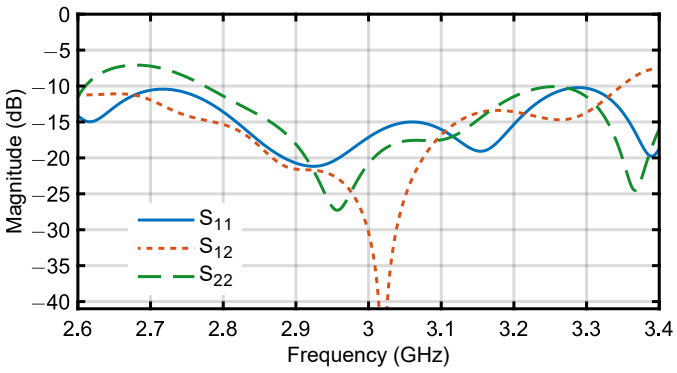

(a)

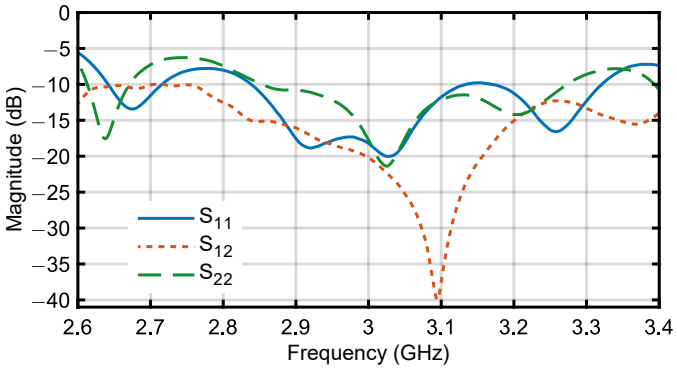

(b)

Fig. 9. (a) Simulated and (b) measured scattering parameters of the compressive array.

B. Subarray Pattern Results

Fig. 10 shows the desired, simulated, and measured subarray patterns at 3 GHz. The desired subarray patterns are those resulting from the compressive-array design algorithm. Between $\theta \in [-20°, 20°]$, the simulated patterns match the desired patterns to within 0.9 dB, and the manufactured patterns match the desired patterns to within 1.5 dB. The simulated subarray sidelobes have peak values within 0.9 dB of the desired subarray sidelobe levels, and the measured patterns have subarray sidelobe levels within 2.6 dB of the desired levels. These results show that there is good agreement with the desired patterns at both the simulation and manufacturing stages of the design process, especially in the main-lobe regions where the gains are the highest.

Simulated subarrays 1 and 2 had peak realised gains in the azimuth plane of 6.9 dBi and 6.1 dBi, respectively. Both manufactured subarrays had peak realised azimuth gains of 7.3 dBi. The subarray sidelobes in the region outside $\theta \in [-90°, 90°]$ were below −12.1 dB and −14.5 dB for the

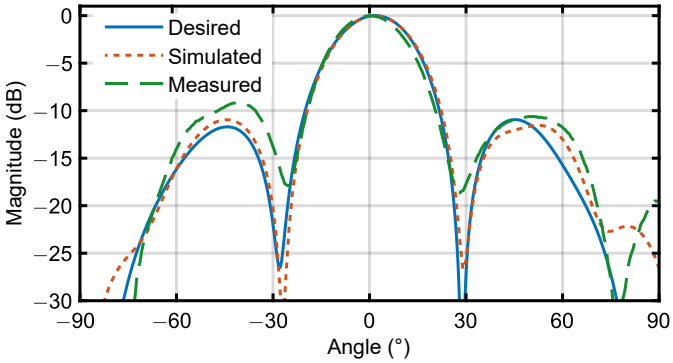

(a)

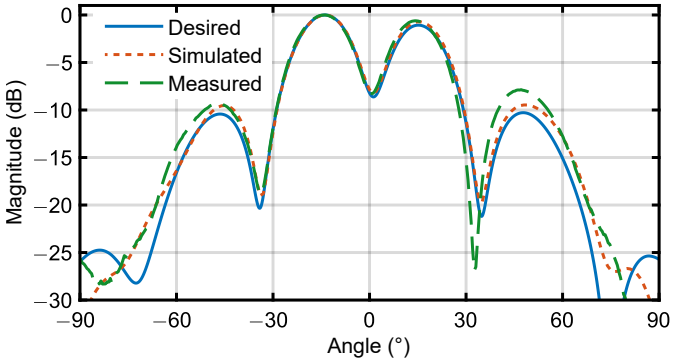

(b)

Fig. 10. Normalised desired, simulated, and measured radiation patterns at 3 GHz for (a) subarray 1 and (b) subarray 2.

simulated and manufactured arrays, respectively. This validates the assumption that the patterns outside $\theta \in [-90°, 90°]$ are sufficiently suppressed to have a negligible effect on the SLL.

The gains of both simulated subarrays were 1.9 dB lower than their respective directivities (over full three-dimensional space), translating to subarray antenna efficiencies of 65%.

C. Steered-Pattern Results at 3 GHz

The steered patterns were obtained by re-calculating the subarray correction weights [5] to minimise the maximum SLL across the steering range at 3 GHz, then combining the corrected subarray patterns numerically with the appropriate beamforming weights [4]. Alternatively, the correction weights could also be calibrated to minimise steered-beam squint or deviation from the desired subarray patterns.

The theoretical SLL of the feed-network response obtained from the compressive-array design algorithm was −11.3 dB. After synthesising the desired response in a chequered network, the SLL worsened by 0.5 dB to −10.8 dB. Interestingly, subsequently implementing the chequered network in microstrip and simulating the complete compressive array resulted in an SLL of −11.2 dB, within 0.1 dB of the theoretical SLL. The manufactured compressive array had an SLL within 1.1 dB of the theoretical SLL at 3 GHz.

Fig. 11 shows the SLLs of the steered patterns as functions of steering angle. The theoretical and simulated arrays have their worst SLLs near broadside, whereas the manufactured array has the worst SLL at the extreme steering angles.

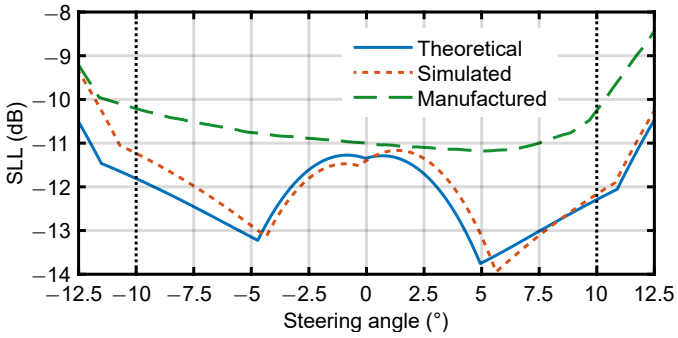

Fig. 11. SLLs as functions of steering angle at 3 GHz.

As expected [4], the SLLs of the arrays start deteriorating rapidly near the extremes of the steering range. The SLL of the manufactured array starts deteriorating rapidly near about +9.5°, which shows the importance of specifying a slightly wider steering range than required.

Although the beamforming weights corresponding to the worst steered pattern for the manufactured array correspond an intended steering angle of −10.1°, the peak of that pattern is in fact at −8.1°. The useful steering range is thus reduced. This squinting effect is analysed further in Section IV-D.

Fig. 12 shows the steered patterns at various steering angles for the theoretical, simulated, and manufactured arrays. In Fig. 12(a), the SLLs near broadside steering for the theoretical and simulated arrays are dominated by the shoulders of the main beams and not the sidelobes themselves. On the other hand, the SLL of the manufactured array is dominated by its much higher sidelobes, which explains the difference in the shape of the manufactured SLL near broadside steering in Fig. 11. The shapes of the steered patterns, including the deviations in the sidelobes for the simulated and manufactured arrays, resemble the subarray 1 patterns in Fig. 10(a), since the contribution of subarray 1 at broadside is far greater than the contribution of subarray 2 (Fig. 10(b)). This illustrates the importance of accurate realisation of the subarray patterns, including the sidelobes outside the steering range, in order to control the sidelobes in the steered patterns.

In Fig. 12(b), at the extreme steering angle of −10.1°, squint (Section IV-D) is at its worst. In Fig. 12(c), at the steering angle of 5°, the SLL of the theoretical array is at its best. In all three cases in Fig. 12, the effect of the manufactured-subarray sidelobes can be observed in the elevated steered-pattern sidelobes.

Fig. 13 shows the steered-pattern 3-dB beamwidths at the various stages of the design process. Also shown are the beamwidths achieved by the simulated four-element dipole array with uniform excitations. The four-element ULA is included since compressive arrays aim to approach the performance of ULAs with the same number of elements over a particular steering range, but with a reduced number of controls. The simulated uniform-excitation ULA had an SLL of −11.6 dB, which is comparable to that of the compressive array. At all stages, the compressive-array beamwidth peaks near broadside steering and is the lowest at the extreme steering angles. The theoretical array has a worst-case beamwidth

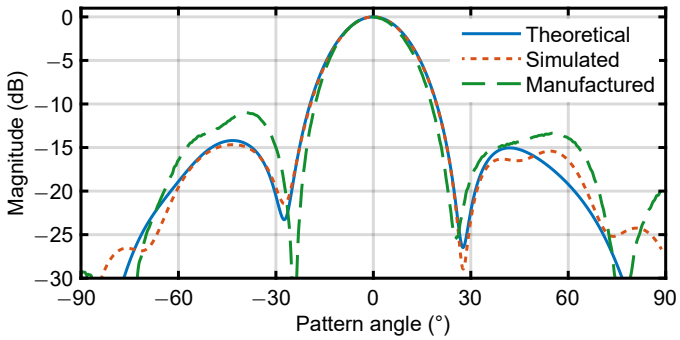

(a)

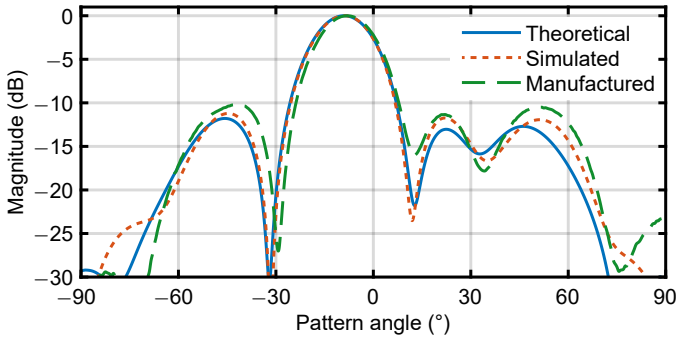

(b)

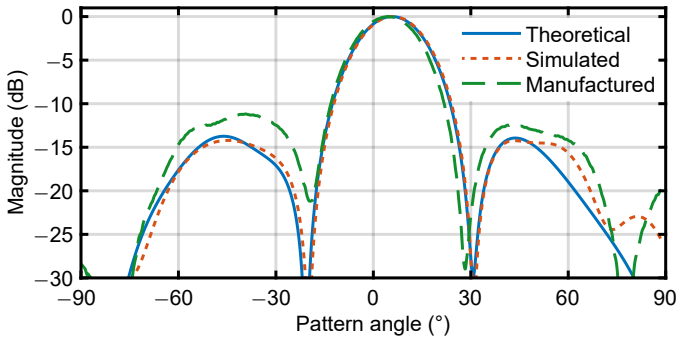

(c)

Fig. 12. Steered patterns at 3 GHz at steering angles of (a) 0°, (b) −10.1°, and (c) 5°.

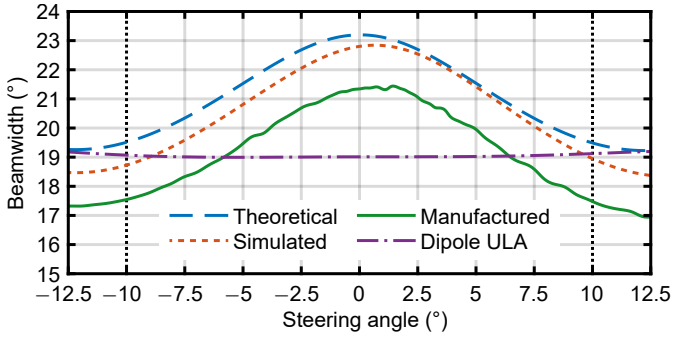

Fig. 13. Beamwidths as functions of steering angle at 3 GHz. The four-element ULA is the simulated dipole array with uniform excitations.

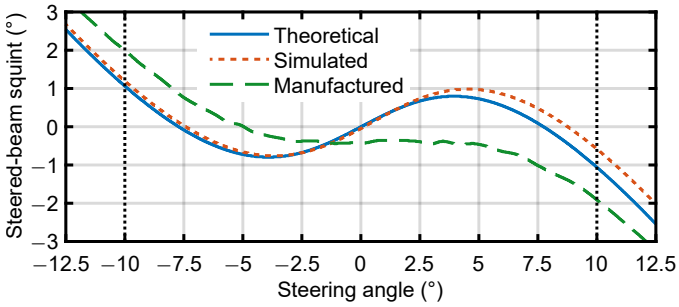

(a)

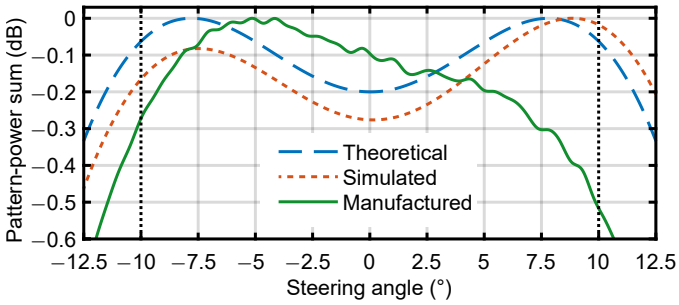

(b)

Fig. 14. Squint analysis: (a) Main-beam squint at 3 GHz. (b) Normalised sums of subarray pattern powers/squared steering-vector norms at 3 GHz.

of 23.2°; the simulated array, 22.8°; the manufactured array, 21.4°; and the conventional ULA, 19.2°. The simulated array has marginally narrower beamwidths than the theoretical array, and the widest beamwidth of the manufactured array is 7.8% better than that of the theoretical array. Even with only half the number of controls, the widest beamwidth of the simulated compressive array is within 18.8% of that of the simulated four-element dipole array with uniform excitations.

D. Squint Analysis at 3 GHz

Fig. 14(a) shows the squints of the steered beams at 3 GHz as functions of steering angle, where squint represents the deviation in the realised pattern peak (the actual direction of the main beam) compared to the intended steering angle. To accurately determine the locations of the pattern peaks, measurement noise was removed by filtering the steered patterns with second-order Savitzky-Golay filters with frame lengths of 30° [32].

The theoretical, simulated, and manufactured arrays have maximum absolute squints of 1.1°, 1.2°, and 2° across the steering range, respectively. This means that the useful steering ranges are reduced by up to 1.1°, 1.2°, and 2° on each side, respectively. For example, in order to realise a steered-beam peak at −8.1° for the manufactured array, the steering weights corresponding to a steering angle of −10.1° must be applied.

The direction of the main beam is maintained at the desired steering angle by means of the constant-subarray-power-sum constraints [4, eq. (15)–(16)]. The sum of the subarray pattern powers is the squared norm of the steering vector, which needs to remain constant near the intended steering angle in order to control the direction of the main beam [4]. The normalised squared steering-vector norm at various stages of the design is

shown in Fig. 14(b). The squared steering-vector norm for the theoretical array has a range of 0.2 dB as specified, which leads to a maximum absolute squint of 1.1°. The squared steering-vector norm for the simulated array has a range of 0.28 dB, which leads to a slightly larger maximum absolute squint of 1.2°. The squared steering-vector norm for the manufactured array has the largest range of 0.53 dB, leading to a maximum absolute squint of 2°. By comparing Figs 14(a) and 14(b), it can be seen that the steered beams have zero squint where the gradients of the steering-vector norms are zero, e.g. near broadside and ±7.5° for the theoretical array and near −5° for the manufactured array. This validates the assumption that steered patterns have zero squint where the steering-vector norms are locally constant [4].

The constant-steering-vector-norm constraints are only maintained in the steering range to allow the suppression of the subarray patterns in the out-of-scan regions [4]. This out-of-scan suppression occurs at all stages of the design as shown by the suppression of the summed subarray pattern powers outside $|\theta| < 10°$ in Fig. 14(b). At the leftmost steering angle, the left side of the steered beam is suppressed by the subarray patterns, thereby squinting the beam towards the right (a positive squint). This can be seen in Fig. 12(b), where the manufactured beam is suppressed on the left. At the rightmost steering angle, the right side of the steered beam is suppressed by the subarray patterns, squinting the beam towards the left (a negative squint). This also explains the decreased beamwidths at extreme steering angles as seen in Fig. 13. In the case of the manufactured array, the suppression of the subarray patterns occurred prematurely within the steering range, leading to worse squint than expected. The steep gradients in the subarray patterns at the extremes of the steering range means that small deviations during manufacturing can cause large deviations in beamforming performance. To account for these deviation as a result of manufacturing tolerances, it is advisable to keep the subarray gains high across a range slightly wider than the specified steering range to avoid premature suppression of the subarray patterns.

V. Conclusion

The design and analysis of the first successfully manufactured chequered-network compressive array with integrated antenna elements has been presented. The practical feasibility of compressive arrays has been demonstrated by this proof of concept, and practical design considerations have been identified.

Only the chequered-network tiles required optimisation in full-wave simulation, making the proposed procedure for implementing chequered networks in microstrip computationally scalable. The use of embedded antenna-element patterns confirmed that the compressive-array design algorithm does not require the assumption of identical element patterns. Good agreement was observed between the theoretical, simulated, and measured results for the assembled compressive array. The prototype had acceptable impedance and isolation bandwidths for a narrowband application.

It was found that deviations in steered-beam squint during manufacturing is a much greater issue than previously assumed, primarily due to the steep gradients in the subarray patterns at extreme steering angles. It is advisable that a slightly wider steering range than required be specified during the design stage, and that subarray gains are kept high across an even wider range to avoid excessive beam squinting.

References

[1] H. E. A. Laue, "Design of Compressive Antenna Arrays," Ph.D. dissertation, Univ. Pretoria, Pretoria, South Africa, 2020.

[2] R. J. Mailloux, *Phased Array Antenna Handbook*. Norwood, MA, USA: Artech House, 2005.

[3] J. S. Herd and M. D. Conway, "The evolution to modern phased array architectures," *Proc. IEEE*, vol. 104, no. 3, pp. 519–529, Mar. 2016.

[4] H. E. A. Laue and W. P. du Plessis, "Numerical optimization of compressive array feed networks," *IEEE Trans. Antennas Propag.*, vol. 66, no. 7, pp. 3432–3440, Jul. 2018.

[5] H. E. A. Laue and W. P. du Plessis, "A checkered network for implementing arbitrary overlapped feed networks," *IEEE Trans. Microw. Theory Techn.*, vol. 67, no. 11, pp. 4632–4640, Nov. 2019.

[6] R. J. Mailloux, *Electronically Scanned Arrays*. San Rafael, CA, USA: Morgan and Claypool Publishers, 2007.

[7] S. P. Skobelev, *Phased Array Antennas with Optimized Element Patterns*. Norwood, MA, USA: Artech House, 2011.

[8] M. I. Skolnik, J. W. Sherman, III, and F. C. Ogg, Jr, "Statistically designed density-tapered arrays," *IEEE Trans. Antennas Propag.*, vol. 12, no. 4, pp. 408–417, Jul. 1964.

[9] W. P. M. N. Keizer, "Linear array thinning using iterative FFT techniques," *IEEE Trans. Antennas Propag.*, vol. 56, no. 8, pp. 2757–2760, Aug. 2008.

[10] R. L. Haupt, "Thinned arrays using genetic algorithms," *IEEE Trans. Antennas Propag.*, vol. 42, no. 7, pp. 993–999, Jul. 1994.

[11] Y. T. Lo, "Aperiodic Arrays," in *Antenna Handbook*, Y. T. Lo and S. W. Lee, Eds. New York, NY, USA: Van Nostrand Reinhold Company Inc., 1988, ch. 14, pp. 14-1–14-37.

[12] V. Murino, A. Trucco, and A. Tesei, "Beam pattern formulation and analysis for wide-band beamforming systems using sparse arrays," *Signal Process.*, vol. 56, no. 2, pp. 177–183, Jan. 1997.

[13] J. S. Herd, S. M. Duffy, and H. Steyskal, "Design considerations and results for an overlapped subarray radar antenna," in *IEEE Aerosp. Conf.*, Big Sky, USA, 5–12 Mar. 2005, pp. 1087–1092.

[14] J. Steckel, D. Laurijssen, A. Schenck, N. BniLam, and M. Weyn, "Low-cost hardware platform for angle of arrival estimation using compressive sensing," in *Eur. Conf. Antennas Propag.*, London, UK, 9–13 Apr. 2018.

[15] Z. Kachwalla, "A limited-scan linear array using overlapping subarrays," *J. Elect. Electron. Eng., Australia*, pp. 126–131, Jun. 1983.

[16] J. Hirokawa and N. J. G. Fonseca, "Generalized one-dimensional parallel switching matrices with an arbitrary number of beams," *IEEE J. Microw.*, vol. 1, no. 4, pp. 975–988, Oct. 2021.

[17] H. Southall and D. McGrath, "An experimental completely overlapped subarray antenna," *IEEE Trans. Antennas Propag.*, vol. 34, no. 4, pp. 465–474, Apr. 1986.

[18] S. M. Duffy, D. D. Santiago, and J. S. Herd, "Design of overlapped subarrays using an RFIC beamformer," in *IEEE Antennas Propag. Soc. Int. Symp.*, Honolulu, USA, 9–15 Jun. 2007, pp. 1949–1952.

[19] M. Ibrahim, V. Ramireddy, A. Lavrenko, J. König, F. Römer, M. Landmann, M. Grossmann, G. Del Galdo, and R. S. Thomä, "Design and analysis of compressive antenna arrays for direction of arrival estimation," *Signal Process.*, vol. 138, pp. 35–47, Sep. 2017.

[20] H. E. A. Laue and W. P. du Plessis, "Compressive direction-finding antenna array," in *IEEE-APS Topical Conf. Antennas Propag. Wireless Commun. (APWC)*, Cairns, Australia, 19–23 Sep. 2016, pp. 158–161.

[21] Y. Wang, G. Leus, and A. Pandharipande, "Direction estimation using compressive sampling array processing," in *IEEE/SP Work. Stat. Signal Process.*, Cardiff, UK, 31 Aug.–3 Sep. 2009, pp. 626–629.

[22] E. Juárez, M. A. Panduro Mendoza, D. H. Covarrubias, A. R. Maldonado, B. Sanchez, and C. del Rio, "An innovative way of using coherently radiating periodic structures for phased arrays with reduced number of phase shifters," *IEEE Trans. Antennas Propag.*, vol. 70, no. 1, pp. 307–316, Jan. 2022.

[23] T. N. Kaifas and J. N. Sahalos, "On the design of a single-layer wideband Butler matrix for switched-beam UMTS system applications [Wireless corner]," *IEEE Antennas Propag. Mag.*, vol. 48, no. 6, pp. 193–204, Dec. 2006.

[24] D. Jaisson, "Fast design of a printed dipole antenna with an integrated balun," *IEE Proc. Microw., Antennas and Propag.*, vol. 153, no. 4, pp. 389–394, Aug. 2006.
[25] R. Li, T. Wu, B. Pan, K. Lim, J. Laskar, and M. M. Tentzeris, "Equivalent-circuit analysis of a broadband printed dipole with adjusted integrated balun and an array for base station applications," *IEEE Trans. Antennas Propag.*, vol. 57, no. 7, pp. 2180–2184, Jul. 2009.
[26] S. M. Sherman and D. K. Barton, *Monopulse Principles and Techniques*. Norwood, MA, USA: Artech House, 2011.
[27] N. Fonseca, "Discussion on reciprocity, unitary matrix, and lossless multiple beam forming networks," *Int. J. Antennas Propag.*, vol. 2015, pp. 1–9, Apr. 2015.
[28] Y. Aslan, A. Roederer, N. J. G. Fonseca, P. Angeletti, and A. Yarovoy, "Orthogonal versus zero-forced beamforming in multibeam antenna systems: Review and challenges for future wireless networks," *IEEE J. Microw.*, vol. 1, no. 4, Oct. 2021.
[29] "RO4000® series – High frequency circuit materials," Rogers Corp., Chandler, USA, Tech. Rep., Pub. 92-004, 2018.
[30] P. L. D. Abrie, *The Design of Impedance-Matching Networks for Radio-Frequency and Microwave Amplifiers*. Dedham, MA, USA: Artech House, 1985.
[31] *Qualification and Performance Specification for Rigid Printed Boards*, IPC-6012 Rev. D Amend 1, Oct. 2017.
[32] S. J. Orfanidis, *Introduction to Signal Processing*. Englewood Cliffs, NJ, USA: Prentice-Hall, 1996.

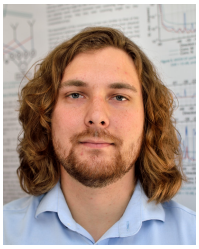

Heinrich Laue (S'16–M'21) received the B.Eng. (Electronic) and B.Eng.Hons. (Electronic) degrees, both with distinction, from the University of Pretoria, South Africa in 2015 and 2016, respectively. He received the Ph.D. (Engineering) degree from the same university in 2020. He currently serves as an IEEE Antennas and Propagation Society Young Professional Ambassador for the year 2022.

Since 2019, he has been with Namibia Water Corporation Ltd as a communications engineer. He is a registered as a Professional Engineer with the Engineering Council of Namibia as well as the Engineering Council of South Africa. His primary research interests are compressive antenna arrays and codebook optimisation.

Warren du Plessis (M'00–SM'10) received the B.Eng. (Electronic), M.Eng. (Electronic), and Ph.D. (Engineering) degrees from the University of Pretoria in 1998, 2003 and 2010 respectively, winning numerous academic awards including the prestigious Vice-Chancellor and Principal's Medal.

He spent two years as a lecturer at the University of Pretoria, and then joined Grintek Antennas as a design engineer for almost four years, followed by six years at the Council for Scientific and Industrial Research (CSIR). He is an Associate Editor of the IEEE Transactions on Aerospace and Electronic Systems. He is currently a Professor at the University of Pretoria, and his primary research interests are cross-eye jamming and thinned antenna arrays.